Full InGaN red light emitting diodes

A. Dussaigne, F. Barbier, B. Damilano, S. Chenot, A. Grenier, A. M Papon, B. Samuel, B. Ben Bakir, D. Vaufrey, J. C Pillet, et al.

Full InGaN red light emitting diodes

A. Dussaigne[1]*, F. Barbier[1], B. Damilano[2], S. Chenot[2], A. Grenier[1], A. M. Papon[1], B. Samuel[1], B. Ben Bakir[1], D. Vaufrey[1], J.C. Pillet[1], A. Gasse[1], O. Ledoux[3], M. Rozhavskaya[3], D. Sotta[3]

[1] *University of Grenoble-Alpes, CEA, LETI, Minatec Campus, F-38054 Grenoble, France*

[2] *CRHEA-CNRS, 06560 Valbonne, France*

[3] *Soitec S.A., 38190 Bernin, France*

Abstract

The full InGaN structure is used to achieve red light emitting diodes (LEDs). This LED structure is composed of a partly relaxed InGaN pseudo-substrate fabricated by Soitec, namely InGaNOS, a n-doped buffer layer formed by a set of $In_xGa_{1-x}N$/GaN superlattices, thin $In_yGa_{1-y}N/In_xGa_{1-x}N$ multiple quantum wells, and a p doped $In_xGa_{1-x}N$ area. p-doped InGaN layers are first studied to determine the optimal Mg concentration. In the case of an In content of 2%, an acceptor concentration of $1x10^{19}/cm^3$ was measured for a Mg concentration of $2x10^{19}/cm^3$. Red electroluminescence was then demonstrated for two generations of LEDs, including chip sizes of 300x300 and 50x50 µm². The differences between these two LED generations are detailed. For both devices, red emission with a peak wavelength at 620 nm was observed for a pumping current density of 12 A/cm². Red light-emission is maintained over the entire tested current range. From the first to the second LED generation, the maximum external quantum efficiency, obtained in the range of 17 to 40 A/cm², was increased by almost one order of magnitude (factor 9) thanks to the different optimizations.

* Corresponding author: amelie.dussaigne@cea.fr

Keywords: InGaN, red LED, full InGaN structure, InGaNOS, relaxed InGaN pseudo-substrate

INTRODUCTION

For virtual and augmented reality (AR/VR) applications, full color micro-displays with pixel pitch smaller than 10 µm are needed. A high brightness is also necessary and nitrides based micro light emitting diodes (micro-LEDs) have been chosen at the expense of their organic counterpart [1,2]. If the three primary colors can be obtained by combining different type of semiconductor families such as III-nitrides for blue and green emission, and phosphides for red emission, the pick and place technique usually employed to associate on the same platform these two types of material family is no longer suitable due to both the small pixel pitch and the number of pixels recommended to reach a very high density. In addition, at such a pixel size (< 10 µm), the red phosphide micro-LED should have its external quantum efficiency (EQE) drastically reduced due to its long carrier diffusion length and to the high density of surface defects present at the pixel sidewalls when obtained by a top down approach [1]. Then, they are two possibilities: color conversion by combining blue emitting micro-LEDs and a converter such as nanophosphors or quantum dots, or achieve the three primary colors (RGB) with the same material family and in a monolithic approach. To get RGB native colors with the same

material, $In_xGa_{1-x}N$ alloy seems to be the best candidate as it can theoretically cover the whole visible range by tuning its InN mole fraction x. However, a strong material degradation is observed for InN mole fraction higher than 25% in $In_xGa_{1-x}N$/GaN quantum wells (QWs) when grown on a conventional template (*i.e.* a GaN buffer layer on sapphire substrate), which is needed for green and red emission. Indeed, the EQE of nitride based LEDs drops dramatically for emission wavelength beyond 500 nm [3,4]. $In_xGa_{1-x}N$ bulk material with high InN mole fraction is known to be thermodynamically unstable [5]. However, the growth under compressive strain for such kind of alloy with misfitting atoms could help to get an homogeneous alloy, but with a certain limitation, mainly determined by surface segregation effects [6,7,8]. Lymperakis *et al.* [8] have demonstrated that the maximum InN mole fraction x of an $In_xGa_{1-x}N$ layer coherently grown on GaN is 25% regardless of the growth conditions. The compositional pulling effect or the In surface segregation effects are known to limit the In incorporation in the $In_xGa_{1-x}N$ alloy [8,10,11,12]. To at least partly overcome this, the strain should be limited in the LED structure. The use of strain compensated MQWs by inserting, for example, AlGaN interlayers inside the active zone can help to release a part of the strain [13,14,15,16]. But the best solution should be to reduce the strain in the LED structure between the active zone and the buffer layer by employing a relaxed InGaN pseudo-substrate. This would permit to enhance the In incorporation rate [17] while keeping a coherent alloy and improve the internal quantum efficiency (IQE) of the LED active region. This will also reduce the quantum confined Stark effect (QCSE) by reducing the piezoelectric polarization in QWs of same In content [18]. While many trials have been realized to get a relaxed InGaN buffer layer either from a GaN template (GaN buffer layer on sapphire substrate) or a sapphire substrate, no results with high crystalline quality have been demonstrated yet [19-24]. However, M. Abdelhamid *et al.* have recently demonstrated the possibility to get an $In_{0.08}Ga_{0.92}N$ buffer layer almost fully relaxed on a GaN template with a good material quality by using the semi-bulk technique [25,26]. The electrochemical porosification of the GaN layer beneath the InGaN buffer seems also promising [27]. In an other way, a relaxed InGaN pseudo-substrate can be obtained by the Smart Cut approach. This is the case of the InGaNOS substrate (InGaN On Sapphire) fabricated by Soitec. It is obtained from a 200 nm thick InGaN layer grown on a GaN template. Its *a* lattice parameter can vary from 3.190 to 3.207 Å up to now by adapting the In content in the InGaN layer and/or the relaxation process. Its dislocation density is the one of the GaN template used to get the initial InGaN layer (*i.e.* 2×10^8 cm^{-2} for the presented InGaNOS substrates in this paper). Some V-shaped defects are present on its surface but it has been shown that an engineered InGaN/GaN superlattice based buffer layer can manage the filling of these V pits [28]. It has also been demonstrated that the whole visible spectrum can be covered with thin InGaN/InGaN MQWs grown on this substrate, from blue to red emission, until 624 nm [28], by choosing the appropriate *a* lattice parameter and/or by adapting the growth conditions [17]. Then, a new LED structure, called *the full*

InGaN structure, can be grown, starting from a relaxed InGaN pseudo-substrate until a p doped InGaN layer.

In this paper, we will show red electroluminescence characteristics obtained with the full InGaN structure using InGaNOS as the relaxed InGaN pseudo-substrate. Central emission wavelengths around 620 nm at 12 A/cm² were achieved for a 300x300 µm² and a 50x50 µm² LEDs. A study as a function of the Mg concentration in p doped InGaN layers will be also presented.

EXPERIMENT

The InGaNOS substrate is composed of a 120 nm thick $In_xGa_{1-x}N$ seed layer bonded on a buried oxide (BOX) on a sapphire substrate. The seed layer originates from a donor composed of a fully strained 200 nm thick $In_zGa_{1-z}N$ layer grown on a GaN buffer layer on a *c*-plane sapphire substrate. The Smart Cut™ process is then applied to transfer this seed layer on a buried oxide on sapphire. To obtain the relaxation of the layer, it is patterned in mesa of 490x490 µm² size which experience then different thermal annealings. At this step, the preservation of a flat surface implies usually that the mesas are partly relaxed (70%). Otherwise, some buckling phenomenon could appear leading to a wavy surface. A second transfer layer is finally required to get the metal polarity on top of the front surface. Depending of the In content of the donor and on the relaxation process, different *a* lattice parameters can be obtained. Here, we consider InGaNOS substrates with an In content in the $In_zGa_{1-z}N$ seed layer of 8% with a *a* lattice parameter varying from 3.205 to 3.207 Å. The *a* lattice parameter of the final mesas are directly measured by X-ray diffraction (XRD) at grazing incidence. The final surface is epi ready for the growth of III-N devices. More details of the fabrication process can be found elsewhere [1729].

The full InGaN structures were grown by metal organic vapor phase epitaxy (MOVPE) on InGaNOS. All the layers were grown under N_2 ambient. Triethylgallium (TEGa), trimethylindium (TMIn), and NH_3 were used as group III and V precursors, respectively. SiH_4 and biscyclopentadienylmagnesium (Cp_2Mg) were used as Si and Mg dopants, respectively. First, the full InGaN structure was composed of a functional buffer formed by 18x pairs of n-doped $In_xGa_{1-x}N$/GaN superlattices with respective thicknesses of 22 nm and 1.8 nm. The InN mole fraction x of the $In_xGa_{1-x}N$ thin layers was 4%. This buffer layer has the advantage to improve the material quality of the InGaN based overgrown layer and to cover the V pits originated from the InGaNOS substrate [28]. This has also been demonstrated for the growth of thick InGaN layer on GaN template [25,26]. Then, the active zone was implemented with 5x $In_yGa_{1-y}N/In_xGa_{1-x}N$ multiple quantum wells (MQWs) with average well and barrier widths of 2.3 nm and 6 nm, respectively. To increase the InN mole fraction in the wells, the growth temperature was reduced from 860°C to 700°C and the growth rate was increased by a factor of 2. The MQWs are

designed to operate in the red spectral range with a thin well width and are aimed to be the same as those used to demonstrate an internal quantum efficiency (IQE) of 6.5% [28]. More details on the growth conditions can be found elsewhere [28]. The InN mole fraction y in the wells is expected to be 40% ±5% in order to emit in the red range. A 10 nm thick non intentionally doped $In_xGa_{1-x}N$ spacer is inserted between the active zone and the p doped part. Finally, the p doped part is grown on top of the spacer with a 125 nm thick p doped $In_xGa_{1-x}N$ layer (p-InGaN) followed by a 20 nm thick highly p doped $In_xGa_{1-x}N$ layer (p++-InGaN). Note that no electron blocking layer was used for these first red LED structures. Before growing the complete LED structures, a study on the p doped InGaN layers was conducted. Six types of samples were grown on a GaN template and on an InGaNOS substrate with a *a* lattice parameter of 3.205Å (InGaNOS-3.205). Both substrates were co-loaded in the same MOVPE run. Their structure is a p-n junction, composed of the same buffer layer as for the full InGaN structure followed by a 250 nm thick p-InGaN layer of same In content. Except for the type of dopant, the growth conditions of this p-InGaN layer were the same as the InGaN layer of the n doped buffer. The growth temperature was 860°C. The Cp_2Mg flux was varied in the p doped part, from Mg flux x1 to Mg flux /140. Mg flux x1 was defined by the Mg flux used for the usual p-GaN of blue LEDs and reduced according to the growth rate of the InGaN layer. The thickness of the p doped part was increased up to 250 nm in order to be able to measure the acceptor – donor ($N_A - N_D$) concentration, with N_A, the acceptor concentration and N_D, the donor concentration. Then, two LED structures, corresponding to two different LED generations, were achieved on two different InGaNOS substrates. The first LED structure (LED A) was grown on an InGaNOS substrate with a *a* lattice parameter of 3.2056 Å, and corresponds to the first generation, while the second LED structure (LED B) was grown on InGaNOS substrate with a *a* lattice parameter of 3.2069 Å, and corresponds to the second generation. Note that the InGaNOS substrate with a *a* lattice parameter of 3.2056 Å was of lower material quality, principally due to buckling effects occurred on the mesa during the preparation of the InGaNOS substrate. There are also some differences in the structure itself: while structure B has the exact structure described above, structure A has a 15x InGaN/GaN pair buffer layer, a 30 nm thick spacer, no p++-InGaN as the Mg concentration in the p-InGaN was already high (*i.e.* 1×10^{20} cm^{-3}), and the thickness of the p-InGaN layer was 300 nm. The Mg concentration in the p-InGaN of structure B was 3×10^{19} cm^{-3}. In addition, the InN mole fraction x switches from 3% for LED A to 3.5% for LED B, only due to the difference in the *a* lattice parameter of the InGaNOS substrates (*i.e.* higher In incorporation rate with increased *a* lattice parameter [17]) as the buffer layer growth temperatures of the two LED structures have been measured to be the same.

A conventional chip process has then been applied on these two structures with different square mesa sizes (300x300 µm² and 50x50 µm² for structures A and B, respectively) defined by photolithography. A reactive ion etching process was used to get the n type buffer layer, on which a Ti (30 nm)/Al (180

nm)/Ni (30 nm)/Au (200 nm) anode contact was deposited. The contact was annealed under N_2 at 740°C during 30 s. The Ni/Au (200 nm) cathode contact was then deposited on top of the structure in order to get a reflective metallic p contact for wavelengths corresponding to the red. For structure A the Ni thickness was 20 nm while it was 2 nm for structure B. The Ni thickness has been reduced in order to further improve the contact reflectivity. The p-contact was annealed under N_2 at 460°C during 4 mins.

The Mg concentration was measured by secondary ion mass spectrometry (SIMS). The acceptor concentration was determined by the electrochemical capacitance voltage profiling technique (ECV). The surface morphology of the two LED structures was measured by atomic force microscopy (AFM). A photoluminescence (PL) set-up using a 405 nm laser diode was used to measure PL spectra of the two LED structures. High resolution scanning transmission electron microscopy (HRSTEM) was performed on a probe-corrected FEI Themis operated at 200 kV. Bright field images were acquired for structural investigations of the whole LED structures. The LEDs were measured directly on wafer. The electroluminescence (EL) was measured backside through the sapphire wafer using a BWTek spectrometer and a Keithley 2400 source meter.

RESULTS

p-InGaN study

To realize the full InGaN structure, a p doped InGaN layer has to be developed in order to avoid a too high tensile strain in this region, and possibly the formation of cracks. The conventional p doped GaN is thus no longer suitable for such structure because the InGaN substrate is relaxed and therefore the GaN layer should be tensily strained onto this structure. A first parametric study has been conducted to determine the influence of the Mg concentration. As described above, six samples composed of an $In_{0.02}Ga_{0.98}N$ based p-n junction were grown on GaN template with various Mg flux used during the growth of the p doped $In_{0.02}Ga_{0.98}N$ layer. The In content reduced to 2% is due to the growth on GaN template, due to the high compressive strain of InGaN grown on GaN. Fig. 1(a) shows the Mg concentration measured by SIMS as a function of the sample depth. From Mg flux x1 to Mg flux /2, the Mg concentration stays around 3×10^{20} cm^{-3}. The Mg flux is thus too high and the solubility limit of Mg atoms in $In_{0.02}Ga_{0.98}N$ is reached. In addition, the Mg concentration profile is not abrupt. From the Mg flux /2 curve, it seems that a Mg retrodiffusion occurred, probably due to the too high Mg flux but as it is not observed in the case of Mg flux x1, it is probably related to the sample itself. The Mg flux had to be reduced again to observe a decrease of the Mg concentration in the InGaN layer. From Mg flux /6 to Mg flux /140, the Mg concentration is reduced from 2×10^{19} cm^{-3} to 2×10^{17} cm^{-3}. The Mg

concentration profile becomes abrupt with a plateau at the maximum concentration almost through the whole p-InGaN thickness. Without thermal annealing, the samples are already conductive but to get a maximum acceptor concentration, a low temperature thermal annealing is necessary. Fig. 1(b) presents the N_A-N_D concentration profile measured by ECV for a Mg concentration of 2 x 10^{19} cm^{-3}. The profile is not abrupt at the interface with the n doped layer but the plateau is reached only after 80 nm. This is not completely in accordance with the SIMS profile of Fig. 1(a), as previously described, for which the doping profile is abrupt directly at the interface with the n doped part. A N_A-N_D concentration of 1 x 10^{19} cm^{-3} can be achieved in the case of a Mg concentration of 2 x 10^{19}/cm^{-3}. These two values are fully consistent as they are usually associated to get an optimal acceptor concentration in the case of the p doped GaN layer [30,31]. The difference between these two values probably comes from compensation phenomenon as previously reported [32,33,34].However, here, the In content of the p-InGaN is only 2% on GaN template. For increased InN mole fraction x in the p doped $In_xGa_{1-x}N$ layer, the optimal Mg concentration should probably be reduced as the ionization level of Mg will also decrease with the reduced band gap [32,33,35,36]. Note that it will also depend on the enhanced defect density usually observed with the increase of the In content, which could impact the acceptor concentration by compensation effects. For comparison, Fig. 1(c) presents the Mg concentration profile in the case of the p-InGaN layer grown on GaN template and on InGaNOS-3.205Å for a Mg flux /6. The same plateau of Mg concentration at 2 x 10^{19} cm^{-3} is obtained in both cases showing that the Mg incorporation is the same on the both substrates even if the In content has a difference of 1% (the In content is 3% on InGaNOS-3.205 in the p doped InGaN layer). In addition, the profile is even a little more abrupt in the case of the InGaNOS substrate. The N_A-N_D value and the abrupt Mg concentration profile obtained are sufficient to consider the growth of a first full InGaN structure.

Material properties comparison of the two LED structures

The AFM image of Fig. 2(a) shows that a high density of V shaped defects (V pits) is present at the surface of LED A. Large and small diameter V pits are visible. The V pit density is drastically reduced in the case of LED B (Fig. 2(b)). Its V pit density is 2 x 10^8 cm^{-2}, same value as the dislocation density of the substrate. Their diameter ranges from 20 to 200 nm. The difference between the two LED surfaces could be explained by the surface morphology of the substrates themselves (material quality of the donor and buckling effect during the relaxation process of the InGaNOS substrate) and by the higher dislocation density starting from the MQW region for LED A (Fig. 3(c)). The high Mg concentration (> 1 x 10^{20} cm^{-3}) in the p-InGaN layer of LED A could be also at the origin of pyramidal defects, known to appear in highly p doped GaN [37]. Fig. 3(a) presents the full InGaN structure of LED B as described in

the experiment section. The corresponding bright field HRSTEM image of structure B is displayed in Fig. 3(b). It shows the InGaN seed layer of the InGaNOS substrate followed by the 18x pairs of the n doped $In_{0.04}Ga_{0.96}N$/GaN superlattice based buffer layer, the 5x $In_yGa_{1-y}N/In_xGa_{1-x}N$ MQWs and the p doped $In_xGa_{1-x}N$ part. A threading dislocation coming from the substrate is visible on the right part of the image. One additional dislocation is also present in the QWs. Fig. 3(c) displays the same bright field HRSTEM image on LED A. Again some threading dislocations coming from the substrate are visible on the right part of the image. A V pit originates in the p doped part, starting from one of the threading dislocations arising from the InGaN seed layer. All the V pits observed by HRSTEM originate from the p doped region. Some additional dislocations start in the quantum well region with a high density compared to the LED B. In both cases, the presence of additional dislocations in the QWs show that, even with the higher *a* lattice parameter provided by the InGaNOS substrate, the strain is still too high for an expected InN mole fraction of 40% in the $In_yGa_{1-y}N$ wells. An even higher *a* lattice parameter would be necessary to get highly efficient red micro-LEDs, ideally with a in-plane lattice parameter of 3.238 Å, *i.e.* equivalent to an In content of 14%. The idea is to get an equivalent strain state in the red emitting QWs compared to blue QWs grown on GaN. This is in accordance with Sharma *et al.* [38].The large difference in the dislocation density in the QWs of the two LEDs will have evidently a direct impact on their respective IQE. Note also that the InGaNOS substrate of LED A was of lower material quality and that the *a* lattice parameter difference between substrates could both explain this discrepancy. Fig. 4 exhibits a zoom in the MQW region of LED B. The quantum wells are well defined but with some thickness inhomogeneities, probably also due to the strain state of the QWs. Local variations of the in-plane lattice parameter can not also be excluded for the moment. In the case of LED A, the QWs are even more disturbed. By taking the thicker areas of each QW in the case of LED B (LED A), the average well and barrier width are 2.3 nm (resp. 2.4 nm) and 6 nm (resp. 7 nm), respectively.

Electroluminescence characteristics of LED A and LED B

EL spectra at 12 A/cm² are presented in Fig. 5 for the two different LED chip sizes. Light-emission in the red spectral range is observed for both cases. For each LED structures, the central emission wavelength is around 620 nm (623 nm for LED B). The spectrum linewidth is 67 nm and 58 nm for LED A and LED B, respectively. In the insets are shown the pictures of the corresponding LED chip under operation. Note that due to the reflective p contact, the LED chip emits mostly from the backside. The red emission observed on the pictures comes thus from the photon diffusion inside the sapphire substrate and from the p contact edges. The EL spectra as a function of the current density presented on Fig. 6(a) and (b) show that the main contribution stays in the red range from 0.1 to 20 A/cm² for both

structures. For LED A, the main contribution is centered at 632 nm at 0.1 A/cm² and blue shifts until 613 nm at 12 A/cm². From 6 A/cm², two other contributions appear at 490 and 550 nm. This could be related to the presence of MQWs on the semi-polar plane of V pits. This has been confirmed by CL measurements for the contributions emitting around 500 nm (not shown). For LED B, the EL spectrum is characterized by one main peak and a shoulder at longer wavelength. To simplify the data treatment, the central emission wavelength has been taken in the center of the broad peak at PL intensity divided by 2 (*i.e.* at FWHM/2). The main peak is centered at 635 nm at 0.04 A/cm² and blue shifts until 622 nm at 20 A/cm². The shoulder shifts until 667 nm att very low current density and is probably due to deep levels in the InGaN based MQWs. From 8 A/cm², a second peak appears at 490 nm with the same origin as for the LED A. The blue shift observed for the two structures (Fig. 6(c) and (d)) could be attributed at least partly to the screening effect of the internal electric field as it is usually observed for structures grown on GaN on sapphire, and also to band-filling phenomenon. Indeed, although the strain is reduced in the two structures by comparison to a conventional structure of same In content grown on GaN, the internal electric field should be high due to the high In content. From our electron holography measurements on green emitting samples [39], the internal electric field value in the QWs should be close to 3 MV.cm^{-1} for an In content of 40% on InGaNOS-3.205, to be compared to 3.6 MV.cm^{-1} for the same In content on GaN template. Note that these values are not absolute ones but can be compared together. In addition, the In content and thickness inhomogeneities inside the MQWs should have also a strong impact on the emission blueshift. Indeed, the broad FWHMs observed, and this is confirmed by CL mappings, show that the whole spectrum is the result of the convolution of different kinds of contributions. As a function of the applied current, carriers can more or less escape from different types of energy potential barriers and fill new energy levels. Nevertheless, at 0.8 A/cm², the FWHM of LED B is 48 nm at 630 nm [40] which is a true red emission [41]. Chromaticity coordinates from CIE 1931 are x = 0.668 and y = 0.331. Finally, the EQE curve as a function of the current density for the two LED chip sizes is displayed in Fig. 7. In the case of LED A, the EQE increases very slowly with the current density while it rises strongly from 2 A/cm² to 40 A/cm² for LED B. The EQE curve of LED B presents an unsual behaviour : a plateau is observed in the current density range of ~ 0.1-1 A/cm2 and then an increase for a larger current density. The reason of this is not understood yet. The maximum EQE of LED B is reached at 40 A/cm² with a value of 0.09% at 616 nm. For LED A, it is reached at 17 A/cm² with a value of 0.01% at 612 nm. The maximum EQE could be increased to 0.17% at 12 A/cm² if the wavelength is reduced to 600 nm (obtained for the LED B structure on an another InGaNOS substrate with a slightly reduced in-plane lattice parameter). Finally, the maximum EQE is 9 times higher for LED B than for LED A, demonstrating a strong improvement between the two LED generations. This is in accordance with both the reduced dislocation density in the MQWs and the improved conductivity in the p-InGaN layer. The reduction of the V pit density plays also a role by providing a higher emitting

surface. The extraction efficiency should be in addition higher for LED B as the p-InGaN thickness was reduced according to ray optics simulations. Indeed, these simulations underline that several interferences occur in LED such as Llyod's mirror and Perrot-Fabry interferences. These two kinds of interferences can be independently tuned. The Perrot Fabry interference is tuned by the cavity length, in the present case of CC LED, by the length between the anode/p-doped InGaN interface and the substrate/air interface. In contrast, in Llyod's mirror, an interference pattern is produced as a result of the combination of the direct ray and the anode reflected ray emitted from quantum wells. Consequently, tuning the p-doped InGaN thickness allows to match the ray phases and enhances the interference intensity in a preferred direction and for a given wavelength. According to our simulations performed with SiLENSe software, reducing the p-doped InGaN thickness from 300 (LED A) to 125nm (LED B) allows to drastically enhance the LED extraction efficiency in normal direction of the LED stack.

Nevertheless, the EQE values stay very low and is far from the best value, to our knowledge, obtained on GaN using an insertion of AlGaN interlayers in the active zone [14]. In this case, the extraction efficiency was 60% [14]. However, IQE measurements realized on the full LED structure (LED B), *i.e.* with the p-InGaN on top of the structure, show that the IQE is reduced by a factor 4 compared to the structure with only the active zone. But it has not been checked yet how much the 405 nm laser diode used for the measurement is absorbed by the p-InGaN layer. If the IQE value is confirmed, the reduction could be due to a Mg diffusion and/or to the growth temperature of the p-InGaN (860°C compared to 700°C for the MQWs) [42]. Next, the extraction efficiency for such conventional chip process is known to be low. In addition, the Ni/Au p contact is not fully reflective even if the Ni thickness was thin (2 nm). Furthermore, according to simulations based on the finite difference time domain method, some photons are guided in the BOX placed in between the LED structure and the sapphire substrate, leading to an even reduced extraction efficiency compared to the same LED structure and technological process applied on the conventional substrate, *i.e.* GaN buffer on sapphire substrate. The extraction efficiency is finally estimated to be lower than 4%. Further simulations by taking into account the whole sapphire substrate thickness should be done to give a reliable value. Anyway, to increase the extraction efficiency, the sapphire substrate and the BOX should be removed at a first step and replaced by a functional substrate that provide a reflective coating at the backside of the LED structure [43]. With such an integration scheme, combined with an appropriated optical engineering of the epilayer stack, a significant improvement of the global performances is expected.

Journal of Applied Physics

AIP Publishing

CONCLUSION

We have shown that red electroluminescence can be obtained by using the full InGaN structure, with the InGaNOS substrate as the relaxed pseudo-substrate, either on 300x300 or 50x50 µm² chip sizes. The central emission wavelength of the spectra stays in the red range for all the current density range tested. A central emission wavelength of 623 nm is obtained at 12 A/cm² at room temperature with a linewidth of 58 nm for a chip size of 50x50 µm². However, although red emission is obtained, the presence of additional dislocations in the active zone suggests that to get high efficiency a higher in-plane lattice parameter would be necessary. Nevertheless, between two LED generations, for which different parameters have been changed such as the material quality and the in-plane lattice parameter of the InGaNOS substrate, and the Mg concentration of the p-InGaN, the EQE is increased by a factor of 9, showing a room for improvement by ongoing the optimization of the different building blocks of this particular LED structure. Also, the extraction efficiency should be addressed by removing the sapphire substrate and the BOX.

DATA AVAILABILITY

The main data that supports the findings of this study are available within the article. Complementary data that support the findings of this study are available from the corresponding author upon reasonable request.

REFERENCES

[1] F. Olivier, S. Tirano, L. Dupré, B. Avanturier, C. Largeron and F. Templier, J. Lumin. 191, 112 (2017)

[2] S. Zhang, Z. Gong, J. J. D. McKendry, S. Watson, A. Cogman, E. Xie, P. Tian, E. Gu, Z. Chen, G. Zhang, A. E. Kelly, R. K. Henderson, and M.D. Dawson, IEEE Photonics J. 4, 1639 (2012)

[3] M. Auf der Maur, A. Pecchia, G. Penazzi, W. Rodrigues, and A. Di Carlo, Phys. Rev. Lett. 116, 027401 (2016)

[4] B. Damilano and B. Gil, J. Phys. D: Appl. Phys. 48, 403001 (2015)

[5] I-hsiu Ho and G.B. Stringfellow, Appl. Phys. Lett. 69, 2701 (1996)

[6] J. Tersoff, Phys. Rev. Lett. 74, 434 (1995)

[7] A.I. Duff, L. Lymperakis, and J. Neugebauer, Phys. Rev. B 89, 085307 (2014)

[8] A. Dussaigne, B. Damilano, N. Grandjean, and J. Massies, J. Cryst. Growth 251, 471 (2003)

[9] L. Lymperakis, T. Schulz, C. Freysoldt, M. Anikeeva, Z. Chen, X. Zheng, B. Shen, C. Chèze, M. Siekacz, X.Q. Wang, M. Albrecht, and J. Neugebauer, Phys. Rev. Mat. 2, 011601(R) (2018)

[10] Y. Inatomi, Y. Kangawa, T. Ito, T. Suski, Y. Kumagai, K. Kakimoto, and A. Koukitu, Jpn. J. Appl. Phys. 56, 078003 (2017)

[11] M. C. Johnson, E. D. Bourret-Courchesne, J. Wu, Z. Liliental-Weber, D. N. Zakharov, R. J. Jorgenson, T. B. Ng, D. E. McCready, and J. R. Williams, J. Appl. Phys. 96, 1381 (2004)

[12] S. Pereira, M. R. Correia, E. Pereira, K. P. O'Donnell, C. Trager-Cowan, F. Sweeney, and E. Alves, Phys. Rev. B 64, 205311 (2001)

[13] US patent: 5,684,309

[14] J-I. Hwang, R. Hashimoto, S. Saito, and S. Nunoue, Appl. Phys. Express 7, 071003 (2014)

[15] K. Lekhal, B. Damilano, H.T. Ngo, D. Rosales, P. De Mierry, S. Hussain, P. Vennéguès, and B. Gil, Appl. Phys. Lett. 106, 142101 (2015).

[16] T. Doi, Y. Honda, M. Yamaguchi, and H. Amano, Jpn. J. Appl. Phys. 52, 08JB14 (2013)

[17] A. Even, G. Laval, O. Ledoux, P. Ferret, D. Sotta, E. Guiot, I. C. Robin, F. Lévy, and A. Dussaigne, Appl. Phys. Lett. 110, 262103 (2017)

[18] J. Zhang and N. Tansu, J. Appl. Phys. 110, 113110 (2011)

[19] K. Hestroffer, F. Wu, H. Li, C. Lund, S. Keller, J.S. Speck, and U. K. Mishra, Semiconductor science and Tech. 30, 105015 (2015)

[20] T. Yamaguchi, N. Uematsu, T. Araki, T. Honda, E. Yoon, and Y. Nanishi, J. Crys. Growth 377, 123 (2013)

[21] T. Hirasaki, M. Eriksson, Q. T. Thieu, F. Karlsson, H. Murakami, Y. Kumagai, B. Monemar, P. O. Holtz, and A. Koukitu, J. Crys. Growth 456, 145 (2016)

[22] T. Ohata, Y. Honda, M. Yamaguchi, and H. Amano, Jpn. J. Appl. Phys. 52, 08JB11 (2013)

[23] J. Däubler, T. Passow, R. Aidam, K. Köhler, L. Kirste, M. Kunzer, and J. Wagner, Appl. Phys. Lett. 105, 111111 (2014)

[24] K. Pantzas, G. Patriarche, D. Troadec, M. Kociak, N. Cherkashin, M. Hytch, J. Barjon, C. Tanguy, T. Rivera, S. Suresh, and A. Ougazzaden, J. Appl. Phys. 117, 055705 (2015)

[25] M. Abderhamid, J. G. Reynolds, N.A. El-Masry, and S.M. Bedair, J. Cryst. Growth 520, 18 (2019)

[26] T. B. Eldred, M. Abdelhamid, J.G. Reynolds, N.A. El-Masry, J.M. LeBeau, and S.M. Bedair, Appl. Phys. Lett. 116, 102104 (2020)

[27] S. S. Pasayat, C. Gupta, Y. Wang, S. P. DenBaars, S. Nakamura, S. Keller, and U. K. Mishra, Materials 13, 213 (2020)

[28] A. Dussaigne, F. Barbier, B. Samuel, A. Even, R. templier, F. Lévy, O. Ledoux, M. Rozhavskaia, D. Sotta, J. Cryst. Growth 533, 125481 (2020)

[29] A. Dussaigne and D. Sotta, "Bridging the green gap with a new foundation", Compound Semiconductor (July 2017)

[30] A. Dussaigne, B. Damilano, J. Brault, J. Massies, E. Feltin, N. Grandjean, J. Appl. Phys. 103, 013110 (2008)

[31] A. Castiglia, J. F. Carlin, and N. Grandjean, Appl. Phys. Lett. 98, 213505 (2011)

[32] K. Kumakura, T. Makimoto, N. Kobayashi, J. Cryst. Growth 221, 267 (2000)

[33] K. Kamakura, T. Makimoto, and N. Kobayashi, J. Appl. Phys. 93, 3370 (2003)

[34] X. Wang, S-B. Che, Y. Ishitani, and A. Yoshikawa, Appl. Phys. Lett. 90, 201913 (2007)

[35] S. Valdueza-Felip, A. Ajay, L. Redaelli, M. P. Chauvat, P. Ruterana, T. Cremel, M. Jimenez-Rodriguez, K. Kheng, and E. Monroy, Solar Energy Materials & Solar Cells 160, 355 (2017)

[36] B. N. Pantha, A. Sedhain, J. Li, J. Y. Lin, and H. X. Jiang, Appl. Phys. Lett. 95, 261904 (2009)

[37] H. Morkoç, "Handbook of Nitride Semiconductors and Devices, Materials Properties", (2008)

[38] T.K. Sharma and E. Towe, Appl. Phys. Lett. 96, 191105 (2010)

[39] D. Cooper, V. Boureau, E. Robin, A. Even, A. Grenier, F. Barbier, and A. Dussaigne, "Determination of the internal piezoelectric potentials and the In concentration in InGaN based quantum wells grown on relaxed InGaN pseudo-substrate by off-axis electron holography", accepted to Nanotechnology

[40] D. Sotta, E. Guiot, O. Ledoux, S. Chenot, B. Damilano, and A. Dussaigne, "Soitec's Relaxed InGaN Substrates Enable Pure Red Emission for Full-Color Micro LED Displays", LEDinside, (Nov. 2018)

[41] Y. Robin, M. Pristovsek, H. Amano, F. Oehler, R. A. Oliver, and J .C. Humphreys, J. Appl. Phys. 124, 183102 (2018)

[42] D. Queren, M. Schillgalies, A. Avramescu, G. Brüderl, A. Laubsch, S. Lutgen, and U. Strauss, J. Cryst. Growth 311, 2933 (2009)

[43] F. Templier *et al.*, "A Novel Process for Fabricating High-Resolution and Very Small Pixel-pitch GaN LED Microdisplays", SID Display week (2017) http://www.leti-cea.com/cea-tech/leti/english/Pages/What's-On/Events/SID-Display-Week.aspx

Journal of Applied Physics

Figure captions

Fig. 1: Mg concentration profile measured by SIMS for (a) the six samples grown on GaN as function of the Mg flux (from Mg x1 to Mg /140), (b) N_A-N_D and N_D-N_A profiles measured by ECV in the case of Mg flux /6 on GaN template, and (c) the Mg flux /6 in the case of the growth on GaN template and on InGaNOS-3.205.

Fig. 2: 5x5 µm² AFM scans of (a) LED A and (b) LED B

Fig. 3: (a) Scheme of the full InGaN structure in the case of LED B, (b) Cross section bright field HRSTEM image of LED B showing the whole structure according to (a), (c) Cross section bright field HRSTEM image of LED A. The lamella of LED A was observed along the $[10\bar{1}0]$ zone axis with the diffraction vectors $g_1 = 0001$ along the growth axis and $g_2 = 11\bar{2}0$ parallel to the surface. The lamella of LED B was observed along the $[11\bar{2}0]$ zone axis with the diffraction vectors $g_1 = 0001$ along the growth axis and $g_2 = 10\bar{1}0$ parallel to the surface.

Fig. 4: Cross section bright field HRSTEM image in the MQW area of LED B. The observation was done along the $[11\bar{2}0]$ zone axis.

Fig. 5: EL spectrum recorded at 12 A/cm² in the case of (a) LED A, and (b) LED B. Insets are pictures taken from the front face of the respective chip at 12 A/cm². The inset of LED B is reproduced from D. Sotta, E. Guiot, O. Ledoux, S. Chenot, B. Damilano, and A. Dussaigne, "Soitec's Relaxed InGaN Substrates Enable Pure Red Emission for Full-Color Micro LED Displays", LEDinside, (Nov. 2018) [40], with the permission of LEDinside.

Fig. 6: EL spectra as a function of the applied current in the case of (a) LED A, and (b) LED B, and the corresponding plot of the central emission wavelength as a function of the current density for (c) LED A and (d) LED B. The figure 6(d) is reproduced from D. Sotta, E. Guiot, O. Ledoux, S. Chenot, B. Damilano, and A. Dussaigne, "Soitec's Relaxed InGaN Substrates Enable Pure Red Emission for Full-Color Micro LED Displays", LEDinside, (Nov. 2018) [40], with the permission of LEDinside.

Fig. 7: Normalized optical power as a function of the current density in the case of LED A (blue circles) and LED B (red triangles).

Figures

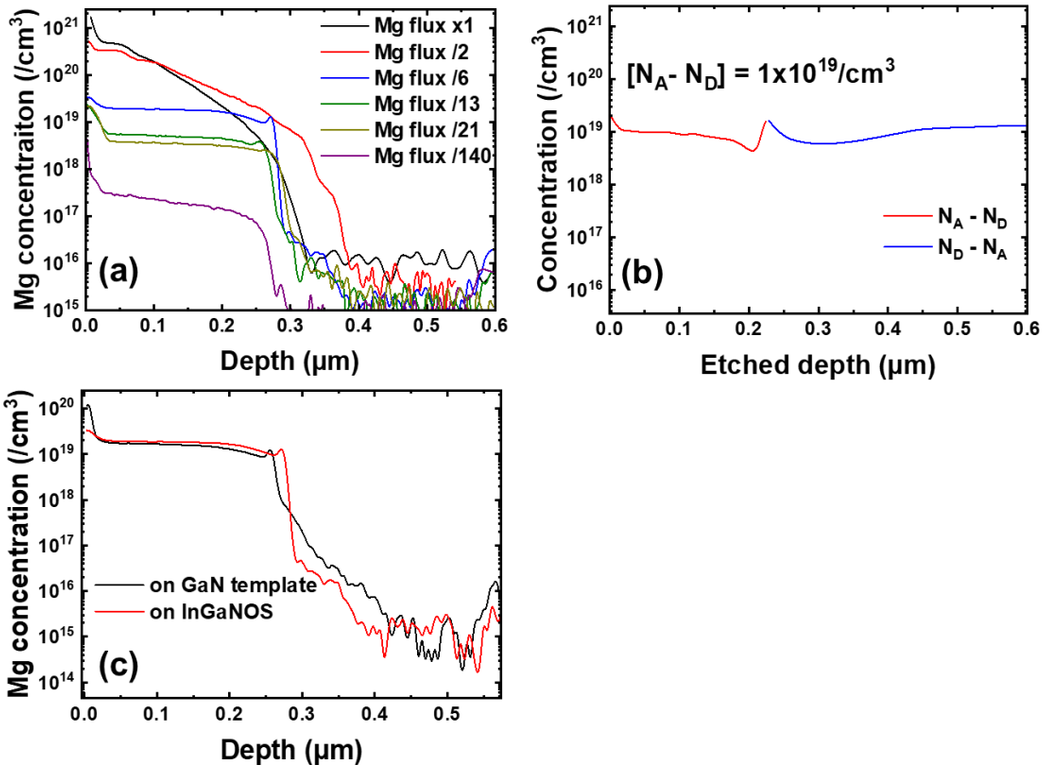

Fig. 1

Journal of Applied Physics

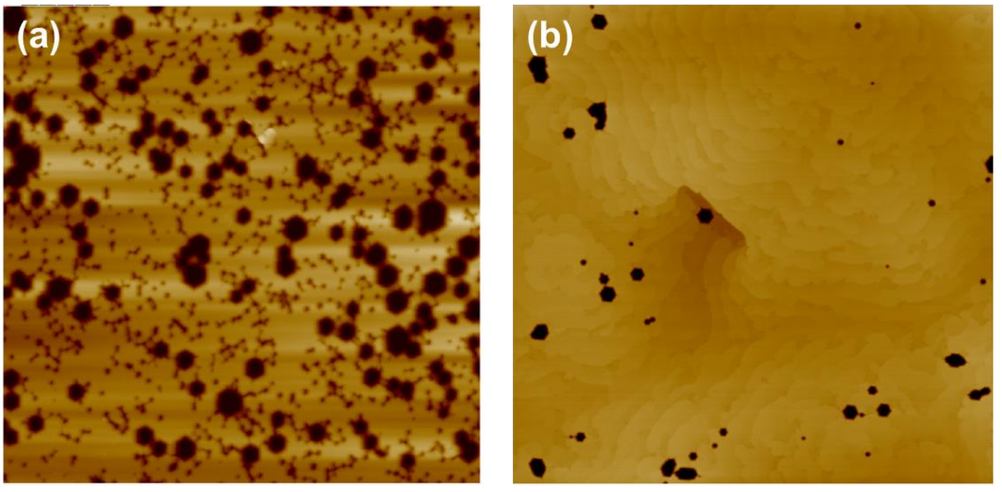

Fig. 2

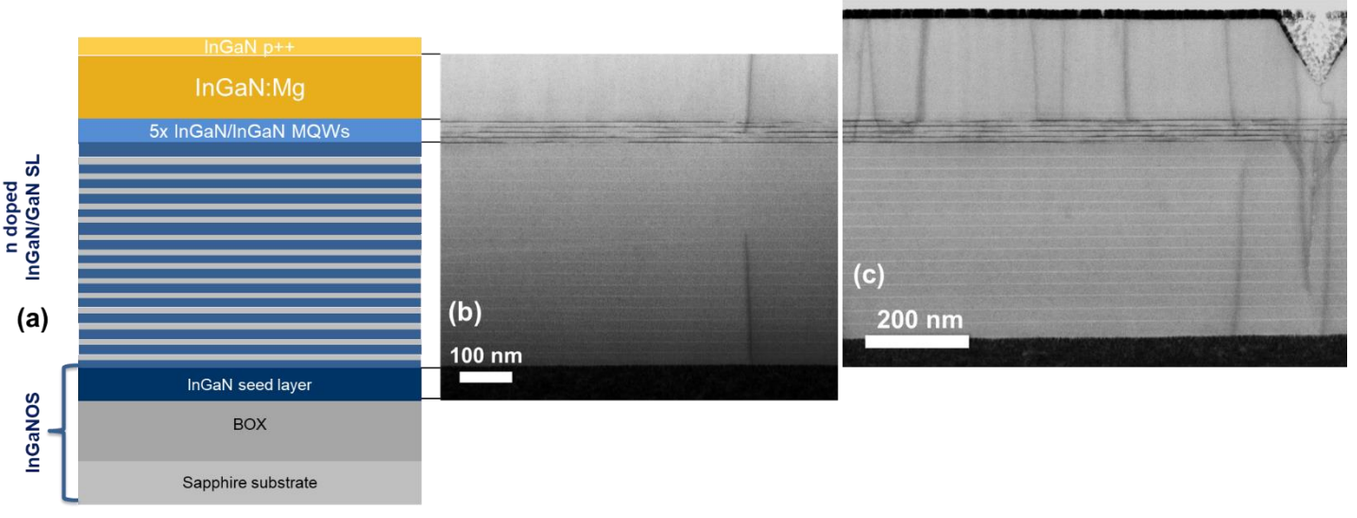

Fig. 3

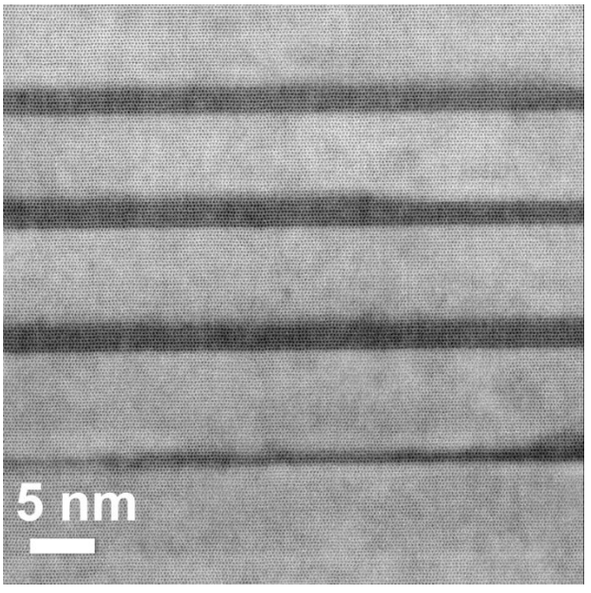

Fig. 4

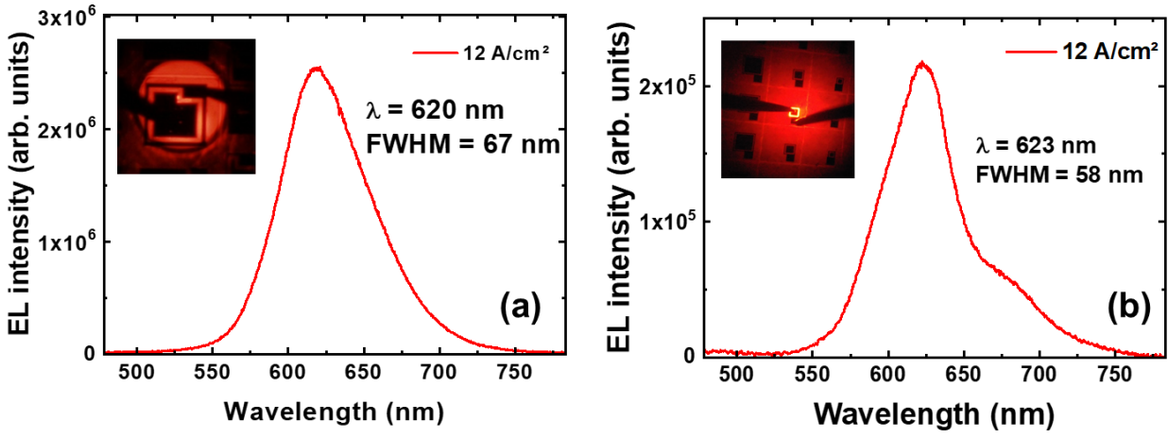

Fig. 5

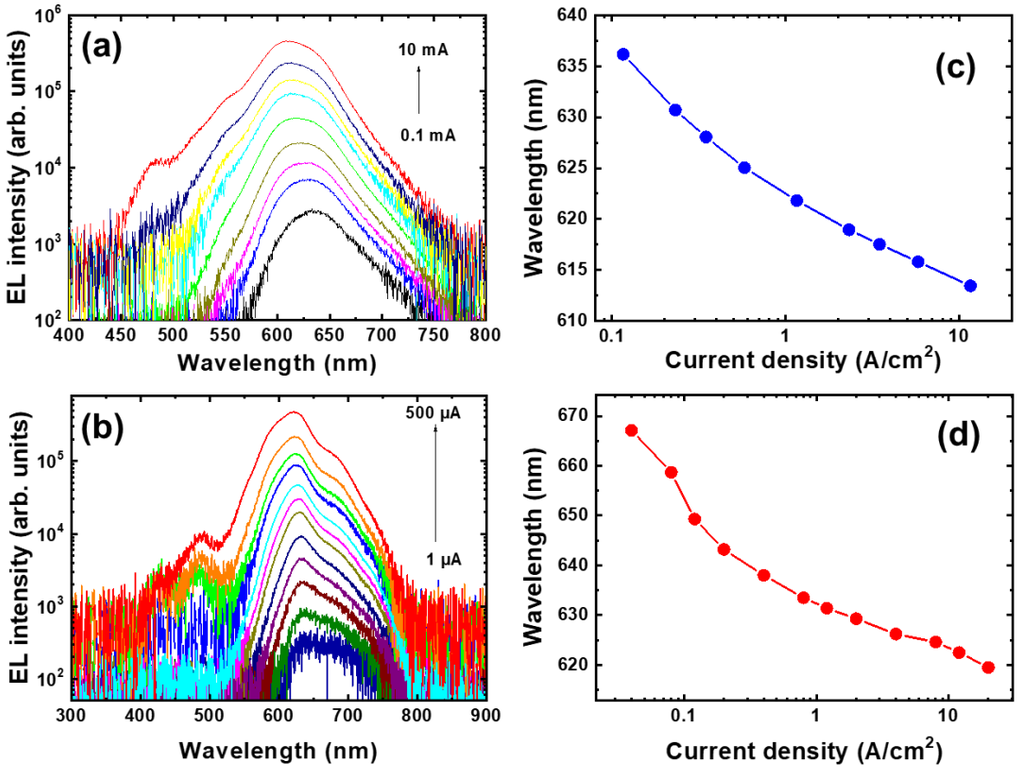

Fig. 6

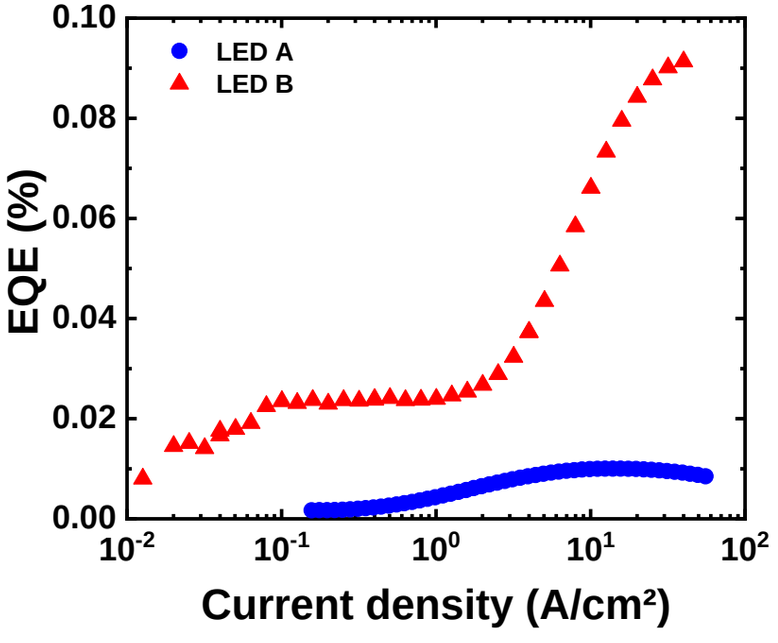

Fig. 7

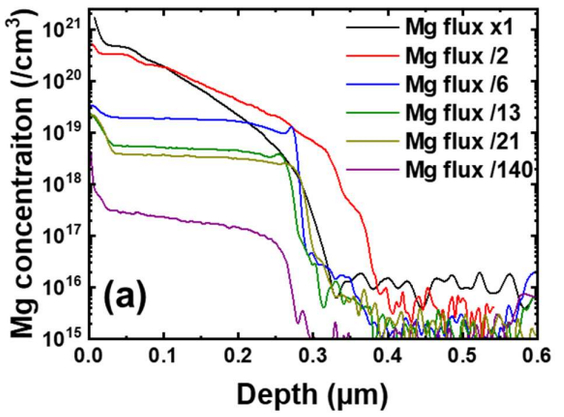

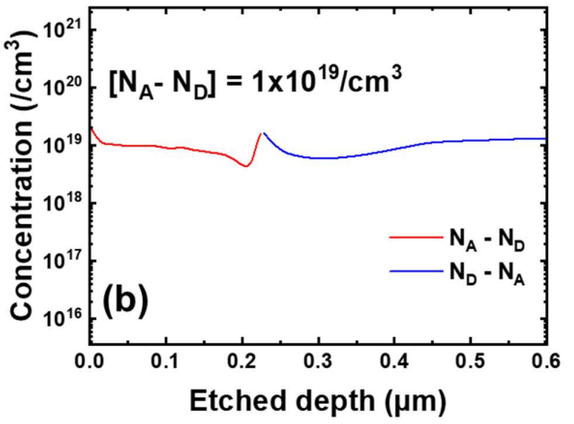

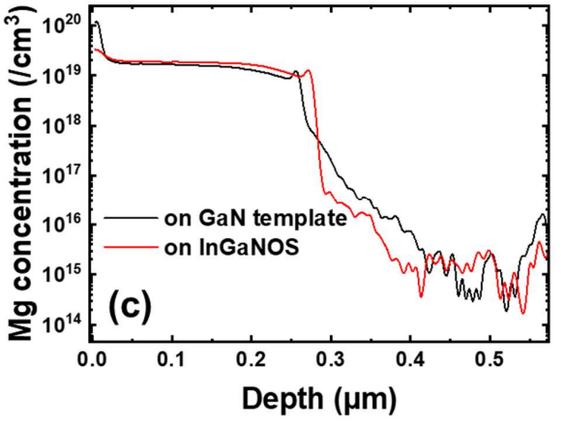

AIP Publishing
Journal of Applied Physics
ACCEPTED MANUSCRIPT

PLEASE CITE THIS ARTICLE AS DOI: 10.1063/5.0016217

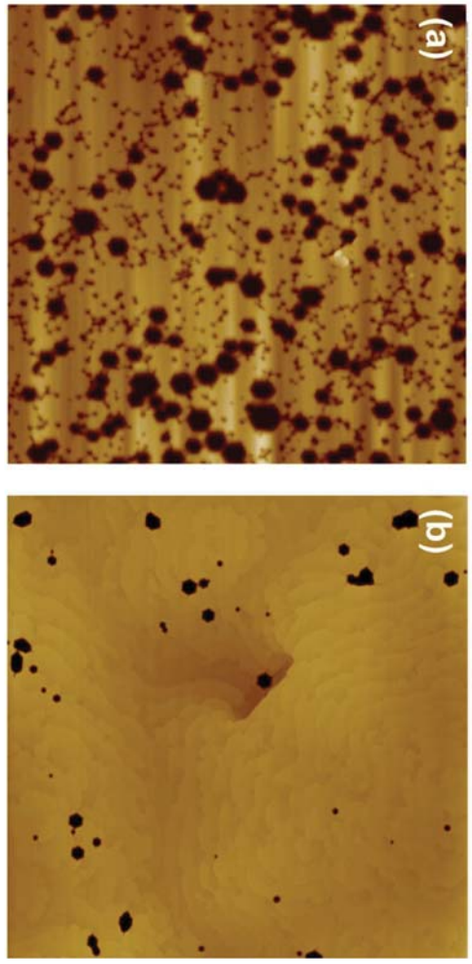

AIP Publishing

Journal of Applied Physics

ACCEPTED MANUSCRIPT

This is the author's peer reviewed, accepted manuscript. However, the online version of record will be different from this version once it has been copyedited and typeset.
PLEASE CITE THIS ARTICLE AS DOI: 10.1063/5.0016217

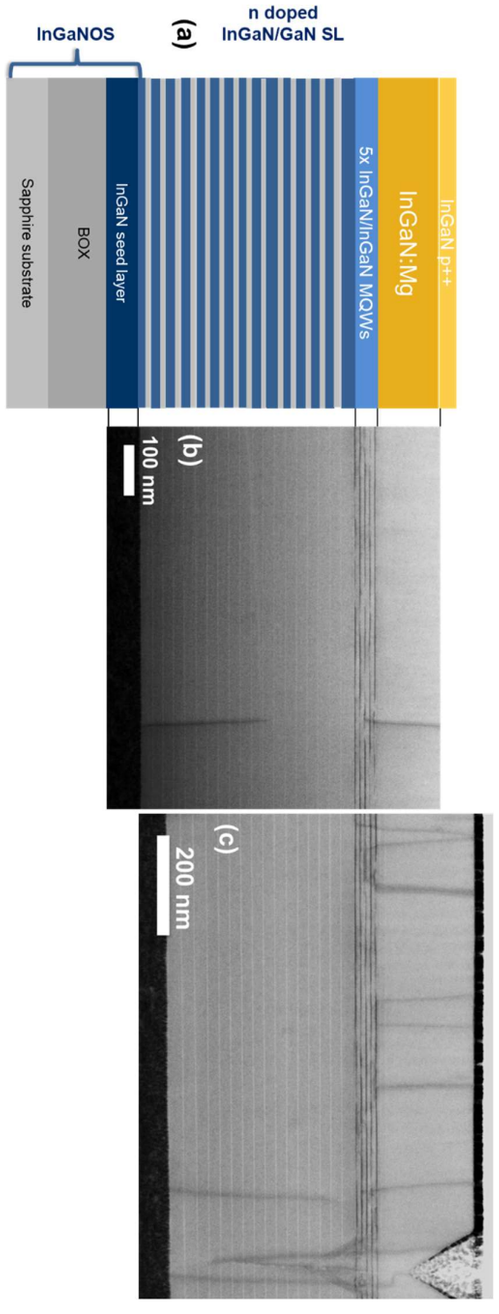

AIP Publishing
Journal of Applied Physics
ACCEPTED MANUSCRIPT

PLEASE CITE THIS ARTICLE AS DOI: 10.1063/5.0016217

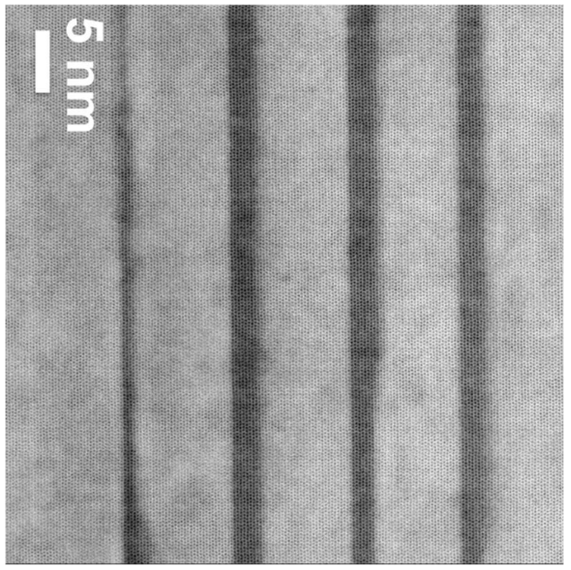

Journal of Applied Physics